

Article

Visualizing Peroxynitrite Fluxes in the Endothelial Cells Reveals the Dynamic Progression of Brain Vascular Injury

Xin Li, Rong-Rong Tao, Ling-Juan Hong, Juan Cheng, Quan Jiang, Ying-Mei Lu, Mei-Hua Liao, Wei-Feng Ye, Nan-Nan Lu, Feng Han, Yong-Zhou Hu, and You-Hong Hu

J. Am. Chem. Soc., **Just Accepted Manuscript** • DOI: 10.1021/jacs.5b06865 • Publication Date (Web): 09 Sep 2015

Downloaded from <http://pubs.acs.org> on September 15, 2015

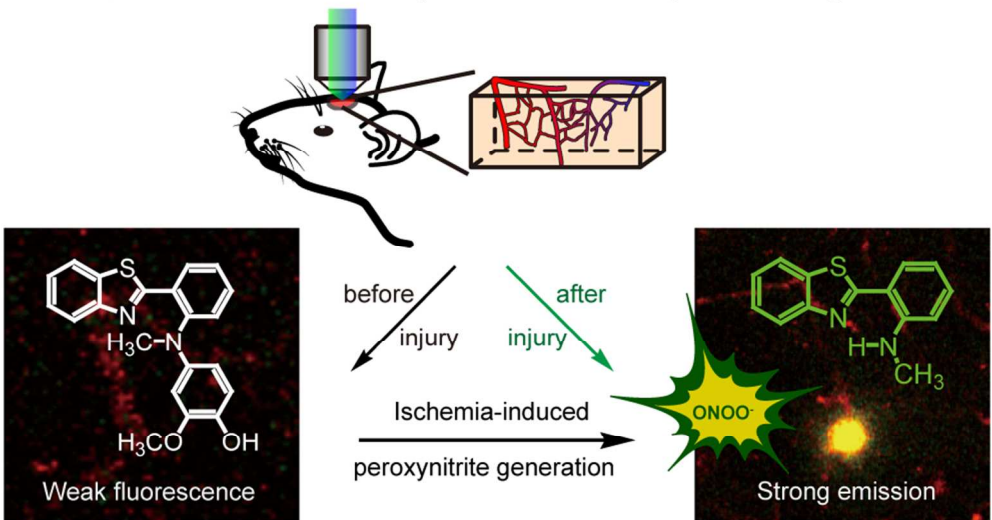
Just Accepted

"Just Accepted" manuscripts have been peer-reviewed and accepted for publication. They are posted online prior to technical editing, formatting for publication and author proofing. The American Chemical Society provides "Just Accepted" as a free service to the research community to expedite the dissemination of scientific material as soon as possible after acceptance. "Just Accepted" manuscripts appear in full in PDF format accompanied by an HTML abstract. "Just Accepted" manuscripts have been fully peer reviewed, but should not be considered the official version of record. They are accessible to all readers and citable by the Digital Object Identifier (DOI®). "Just Accepted" is an optional service offered to authors. Therefore, the "Just Accepted" Web site may not include all articles that will be published in the journal. After a manuscript is technically edited and formatted, it will be removed from the "Just Accepted" Web site and published as an ASAP article. Note that technical editing may introduce minor changes to the manuscript text and/or graphics which could affect content, and all legal disclaimers and ethical guidelines that apply to the journal pertain. ACS cannot be held responsible for errors or consequences arising from the use of information contained in these "Just Accepted" manuscripts.



ACS Publications

Fluorescent Probe for Monitoring Neurovascular Peroxynitrite in Living Mice



84x48mm (300 x 300 DPI)

Visualizing Peroxynitrite Fluxes in the Endothelial Cells Reveals the Dynamic Progression of Brain Vascular Injury

Xin Li,^{†,||} Rong-Rong Tao,^{†,||} Ling-Juan Hong,[‡] Juan Cheng,[†] Quan Jiang,[‡] Ying-Mei Lu,[§] Mei-Hua Liao,[‡] Wei-Feng Ye,[‡] Nan-Nan Lu,[‡] Feng Han,^{*,‡} Yong-Zhou Hu,^{*,†} You-Hong Hu^{*,†}

[†]ZJU-ENS Joint Laboratory of Medicinal Chemistry, College of Pharmaceutical Sciences, Zhejiang University, Hangzhou 310058, China

[‡]Institute of Pharmacology and Toxicology, College of Pharmaceutical Sciences, Zhejiang University, Hangzhou 310058, China

[§]School of Medicine, Zhejiang University City College, Hangzhou 310015, Zhejiang, China

ABSTRACT: Accumulating evidences suggest that the formation of peroxynitrite (ONOO⁻) in the cerebral vasculature contributes to the progression of ischemic damage, while the underlying molecular mechanisms remain elusive. To fully understand ONOO⁻ biology, efficient tools that can realize the real-time tracing of endogenous ONOO⁻ fluxes are indispensable. Although there have been a few ONOO⁻ fluorescent probes reported, a robust probe applicable for the direct visualization of ONOO⁻ fluxes in the cerebral vasculature of live mice is still unavailable. While there are a few ONOO⁻ fluorescent probes reported, direct visualization of ONOO⁻ fluxes in the cerebral vasculature of live mice remains a challenge. Herein, we present a fluorescent switch-on probe (NP3) for ONOO⁻ imaging. NP3 exhibits good specificity, fast response and high sensitivity toward ONOO⁻ both *in vitro* and *in vivo*. Moreover, NP3 is two-photon excitable and readily brain-blood barrier penetrable. These desired photophysical and pharmacokinetic properties endow NP3 the capability to monitor brain vascular ONOO⁻ generation after injury with excellent temporal and spatial resolution. As a proof of concept, NP3 has enabled the direct visualization of neurovascular ONOO⁻ formation in ischemia progression *in vivo* in live mice brain using two-photon laser scanning microscopy. This is the first example of directly visualized ONOO⁻ flux in the living mice brain. Due to these favorable properties, NP3 holds great promise for visualizing endogenous peroxynitrite fluxes in a variety of pathophysiological progressions *in vitro* and *in vivo*.

■ INTRODUCTION

Peroxynitrite (ONOO⁻), a highly reactive nitrogen species generated from the reaction between nitric oxide (NO) and superoxide (O₂⁻) at a diffusion-limited rate of $1.9 \times 10^{10} \text{ M}^{-1} \text{ s}^{-1}$ under pathological conditions,¹ attracts increasing attention due to its "double-edged" character.^{2,3} ONOO⁻ may exert contributory effect by participating in nitrating tyrosine signaling.⁴ Nevertheless, ONOO⁻ is more frequently regarded as deleterious due to its nitrosative damage to lipids, proteins, and DNA.^{5,6} ONOO⁻ has been implicated in various redox-related diseases,^{5,7,8} including ischemia-reperfusion injury.⁹ We have been particularly interested in the roles of ONOO⁻ in the progression of brain ischemia-induced endothelial dysfunction and neurovascular pathogenic cascades. Our preliminary results have shown that ONOO⁻ is formed under conditions of ischemia and that its nitrosative damage is implicated in neurovascular damage following cerebral ischemia.¹⁰⁻¹² In our previous work, ONOO⁻ was primarily detected by immunostaining 3-nitrotyrosine.¹⁰⁻¹² Traditional biology assay for ONOO⁻ primarily relies on the immunostaining of 3-nitrotyrosine.¹³ This method has the major limitation of being incompatible with living systems and can therefore no longer satisfy research needs for tracking native ONOO⁻ in real time

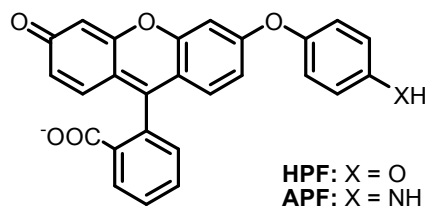
with high spatial resolution, which is pivotal for fully understanding ONOO⁻ pathology in contexts of ischemia *in vivo*.

Fluorescence imaging employing small molecular probes, however, has emerged as a desirable and indispensable tool for interrogating intact living samples.^{14,15} Due to the obvious technical and practical advantages of good membrane-permeability, high sensitivity and operational simplicity, fluorescence probes are attracting increasing attention in life science fields,¹⁶⁻¹⁹ especially those two-photon excitable probes because they are compatible with two-photon fluorescence microscopy and can therefore realize the three-dimensional imaging of biological specimens with deeper tissue penetration and less photodamage.²⁰⁻²² Indeed, several fluorescent probes are commercially available to detect ONOO⁻, such as aminophenyl fluorescein (APF) and hydroxyphenyl fluorescein (HPF).²³ Unfortunately, these probes are limited by their poor selectivity for ONOO⁻ against other highly reactive species, such as •OH or ClO⁻.²⁴ To address this problem, several research groups have set out to develop new probes, and these elegant work have resulted in the development of several selective probes suitable for imaging ONOO⁻ in live cells,²⁵⁻³⁷ live mice,³⁰ or even the redox cycles between ONOO⁻ and glutathione.^{30,32,38} Facilitated by these probes, visualization of ONOO⁻ in macrophages during immune response,²⁵

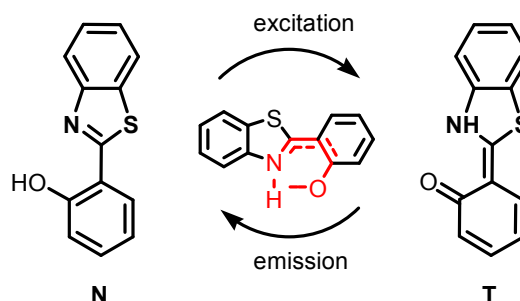
27,29,30,32,33,35 or in mouse hearts under atherosclerosis,²⁶ has been realized. However, none of these probes have realized real-time visualization of ONOO⁻ production in the brain of live animals with ischemia-induced neurovascular damage,

which represents a great challenge in the development of brain imaging agents, ascribing to the rigid requirements. However, study on the real-time visualization of ONOO⁻ production in the brain of live animals with

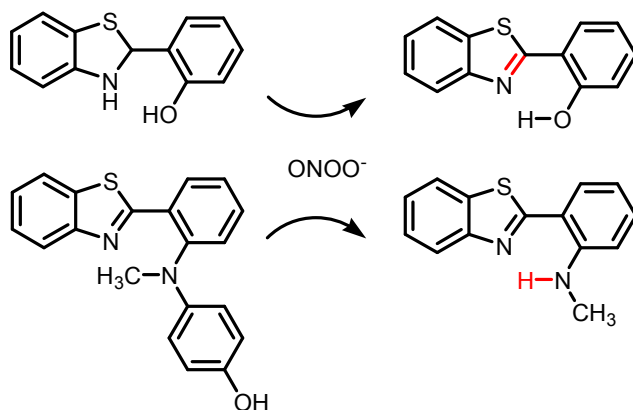
Structures of HPF and APF



ESIPT effect of benzothiazole dyes



Design philosophy



Structures of ONOO⁻ probes

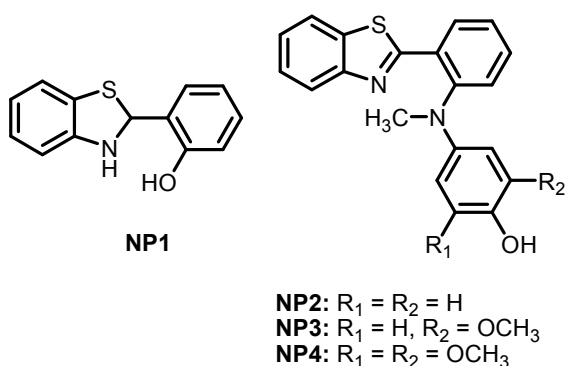


Figure 1. Structures of the BT series of ONOO⁻ probes and our design philosophy.

ischemia-induced neurovascular damage is still lacking, which represents a great challenge ascribing to the rigid requirements for brain imaging agents including high specificity, desired photophysical properties and good blood-brain barrier (BBB) penetrability.^{39,40}

Herein, we report a two-photon fluorescent "switch-on" probe for the detection of ONOO⁻. The probe, judiciously designed by combining the basic principles of fluorescent probe design and drug design, is highly specific and sensitive towards ONOO⁻, two-photon excitable, and most importantly, readily BBB penetrable. It is fluorescence-silent in the absence of ONOO⁻, but can respond rapidly to ONOO⁻ with dramatic emission enhancement (utmost 600-fold). Its capability to track *in situ* generation of ONOO⁻ in live cells and live mice with ischemia-induced neurovascular damage has been fully characterized.

RESULTS AND DISCUSSION

Probe Design and Synthesis. To image ONOO⁻ in live animals, the fluorophore selected for probe construction should be non-toxic, sufficiently bright, inert to other species in the complex biological context, excitable with deep-

penetrating infrared light, and possess desired pharmacokinetic profiles. Among the prevalent fluorescent markers for bio-imaging, 2-(2'-hydroxyphenyl)benzothiazole (BT) provoked our interest due to its drug-like physical-chemical performance and good photophysical properties. First, the benzothiazole skeleton may exhibit the desired pharmacokinetic properties, especially the BBB penetration ability mandatory for brain imaging agents, as exemplified by [¹¹C]PIB, an extensively studied positron emission tomography imaging probe for A β plaques in humans.⁴¹ Second, the BT series of fluorophores commonly exist in the normal form (N) with weak fluorescence but can automerize under excitation (T) *via* a process called "excited state intramolecular proton transfer (ESIPT)" (Figure 1),⁴² accompanied by both an enhancement and red shift of their fluorescence. Blockage of this ESIPT effect with a special chemical motif that can react selectively with intended target in complex biological milieu to initiate the ESIPT process enables the design of sensitive fluorescent probes. Third, BT fluorophore is two-photon excitable and may be compatible for live tissue imaging.⁴³ With all these considerations, probe NP1 was designed by blocking the ESIPT process with a saturated C-N bond (Figure 1). We envisioned that the great tendency to be aromatic would render NP1 susceptible to

oxidation by ONOO^- and therefore restore the ESIPT process. **NP1**, as anticipated, could indeed respond to ONOO^- with a swift fluorescence intensity enhancement in PBS (10 mM, pH 7.4) (Figure S1 and S2). However, **NP1** was found unstable when exposed to air. This instability challenges its selectivity. To develop probes with improved stability and specificity, we next blocked the hydrogen donor of the ESIPT process and designed **NP2** by switching the hydroxyl group to *N*-methyl-*p*-hydroxyl aniline, where the phenol group may be oxidized to benzoquinone by ONOO^- , accompanied by the N-C (sp^2) bond cleavage, thereby furnishing a proton donor (Figure 1).²⁶ **NP3** and **NP4** were also designed by installing electron-donating groups to the *p*-hydroxyl aniline ring in order to make the hydroxyl group more susceptible to oxidants. All the probes were facilely synthesized using Mills reaction (Scheme S1).

Probe Evaluation. We first tested the fluorescence responses of **NP2-4** towards ONOO^- . These probes (5.0 μM) alone were nearly non-emissive in PBS. In contrast, in the presence of ONOO^- (10 μM), all showed obvious fluorescence enhancement, and **NP3** was the most sensitive one with an increase factor of 600-fold, followed by **NP2** and **NP4** (Figure S3). These results not only distinguish **NP3** as a desirable candidate for further study, but suggest that both electronic and steric effects should be considered for probe design because the steric effects of the methoxy groups adjacent to the hydroxyl group in **NP4** greatly outweigh their positive electron-donating effects.

Characterization of the Spectroscopic Response of NP3 towards ONOO^- : Spectroscopic Properties and Selectivity. To profile the response of **NP3** towards ONOO^- in detail, we examined its specificity by recording its responses towards various reactive oxygen species (ROS) and reactive nitrogen species (RNS). Encouragingly, no analytes other than ONOO^- could switch on the fluorescence of **NP3**. **NP3** could still recognize ONOO^- with a dramatic increase in fluorescence intensity even in the presence of other reactive species, cations or amino acids commonly found in biological system, implying the great specificity of **NP3** towards ONOO^- (Figure 2a, Figure S4).

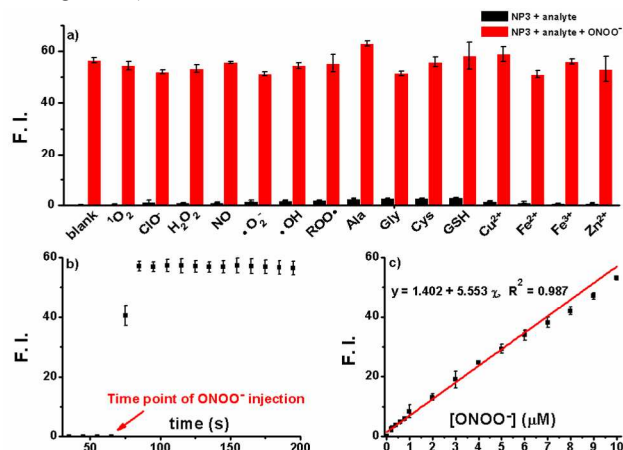


Figure 2. Characterization of the fluorescent response of **NP3** towards ONOO^- . (a) The fluorescent switch-on response of **NP3** was preferentially towards ONOO^- , and the presence of other analytes did not cause interference. Fluorescent responses of **NP3** (5 μM) towards various analytes (10 μM). Data shown represent the fluorescent intensity at 470 nm 30 min after the addition of

various analytes. (b) **NP3** responds to ONOO^- sufficiently fast to reach its maximum intensity within seconds. ONOO^- (final concentration 10 μM) was quickly injected into a solution of **NP3** (final concentration 5 μM) and the fluorescent intensity at 470 nm was plotted against time. (c) The fluorescent readout of the detection reaction was linearly correlated with the concentrations of ONOO^- . Fluorescence enhancement of **NP3** (5 μM) at 470 nm as a function of ONOO^- (0-10 μM) after 15 min of reaction. All the data were acquired in PBS (10 mM, pH 7.4) with excitation 375 nm.

Next, the sensing kinetics was studied, and the reaction between **NP3** and ONOO^- completed within seconds (Figure 2b, Figure S5), which is important given the extremely elusive nature of ONOO^- . Moreover, the fluorescence enhancement of **NP3** was linearly correlated with the concentrations of ONOO^- ranging from 0-10 μM , implying the great potential of **NP3** to quantify ONOO^- (Figure 2c, Figure S6). The detection limit of **NP3** was as low as 5.0 nM (S/N = 3) (Figure S7). Notably, ONOO^- detection by **NP3** was insensitive to pH changes in the surroundings (Figure S8). Additionally, sufficient photostability was observed for both **NP3** and the detection system (Figure S9), indicating the robustness of **NP3**.

We also evaluated the ability of **NP3** to detect ONOO^- in a two-photon excitation mode by measuring the fluorescence spectra of the **NP3-ONOO}^- mixture with two-photon excitation. As expected, sensitive signals retained. under two-photon excitation, and the intensity at 470 nm (λ_{em}) of the mixture excited at 750 nm (or even 800 nm) was comparable to that excited at 400 nm (Figure S13). The two-photon absorption cross sections (σ) of the system at 760-820 nm were also determined with fluorescein in H_2O (pH = 13) as the standard,⁴⁴ and the σ_{max} was observed at 820 nm with a value of 3.6 GM (Figure S10). These results firmly support the feasibility of **NP3** as a highly specific and sensitive probe for ONOO^- *in vitro*, and shows promise for *in vivo* imaging.**

In agreement with the fluorescence switch-on response, treating **NP3** (10 μM) with ONOO^- could also induce a dramatic change in its UV absorption profile. **NP3** itself exhibited a major absorption band centered at 300 nm (ϵ 16310), whereas ONOO^- treatment resulted in the disappearance of this band and the appearance of two new bands centered at 285 nm and 350 nm, both of which strengthened in a ONOO^- concentration-dependent manner (Figure S11), indicating removal of the phenol ring and generation of an intramolecular hydrogen bond as shown in Figure 1. We also verified the detection mechanism by isolating and characterizing the reaction product using ^1H NMR and HRMS spectra analysis (Figure S12, S13).⁴⁵

Determination of Plasma and Brain NP3 Concentrations. Pharmacokinetic study in C57 mice showed that **NP3** readily crossed the brain-blood barrier (Figure S14). A 1.3-fold brain/plasma ratio was achieved after 0.5 h of tail intravenous injection (I. V.) dosing at 10 mg/kg. The absolute brain concentration reached a high level of 970 ng/mL 0.5 h after **NP3** administration and only 136 ng/mL remained after 2 h, indicating the efficient brain penetration and fast brain clearance rate of **NP3**, which are deemed advantageous for brain imaging agents.

Fluorescent Response of NP3 to Dynamic Changes in Nitrosative Stress in Live Endothelial Cells. With the photophysical profiles of NP3 fully characterized, we next investigated its feasibility for dynamically tracking intracellular ONOO⁻ generation. A time-lapse series of single confocal plane images were taken to observe the NP3 fluorescence response towards ONOO⁻ in live EA.hy926 endothelial cells after incubation with or without 3-morpholinosydnonimine (SIN-1, 0.5 mM), an ONOO⁻ donor. As shown in Figure 3, no detectable fluorescence signal was observed in endothelial cells loaded with NP3 in the absence of the ONOO⁻ donor SIN-1 (Figure 3a and b). However, upon exposure to SIN-1, intracellular fluorescence in endothelial cells gradually increased 10 min after SIN-1 stimulation and kept increasing in

a time-dependent manner until at least 50 min after treatment (Figure 3a and b). In contrast, clearance of ONOO⁻ with uric acid (100 μ M) or FeTTPS (1 μ M) blunted the robustness of NP3 fluorescence in ONOO⁻-treated endothelial cells (Figure 3c, Figure S15, S16). NP3 also worked well as an efficient ONOO⁻ probe in other cell lines, as shown in human brain microvascular endothelial cells (HBMEC) in Figure S17. The ONOO⁻ (Figure S17a) or SIN-1 (Figure S17b) treatment-induced NP3 fluorescence elevation was also observed in a dose-dependent manner in HBMEC. These results indicate that NP3 is applicable for real-time tracking of ONOO⁻ generation in live cells and suggest its promise for serving as a molecular imaging tool to explore ONOO⁻ biology under pathological conditions.

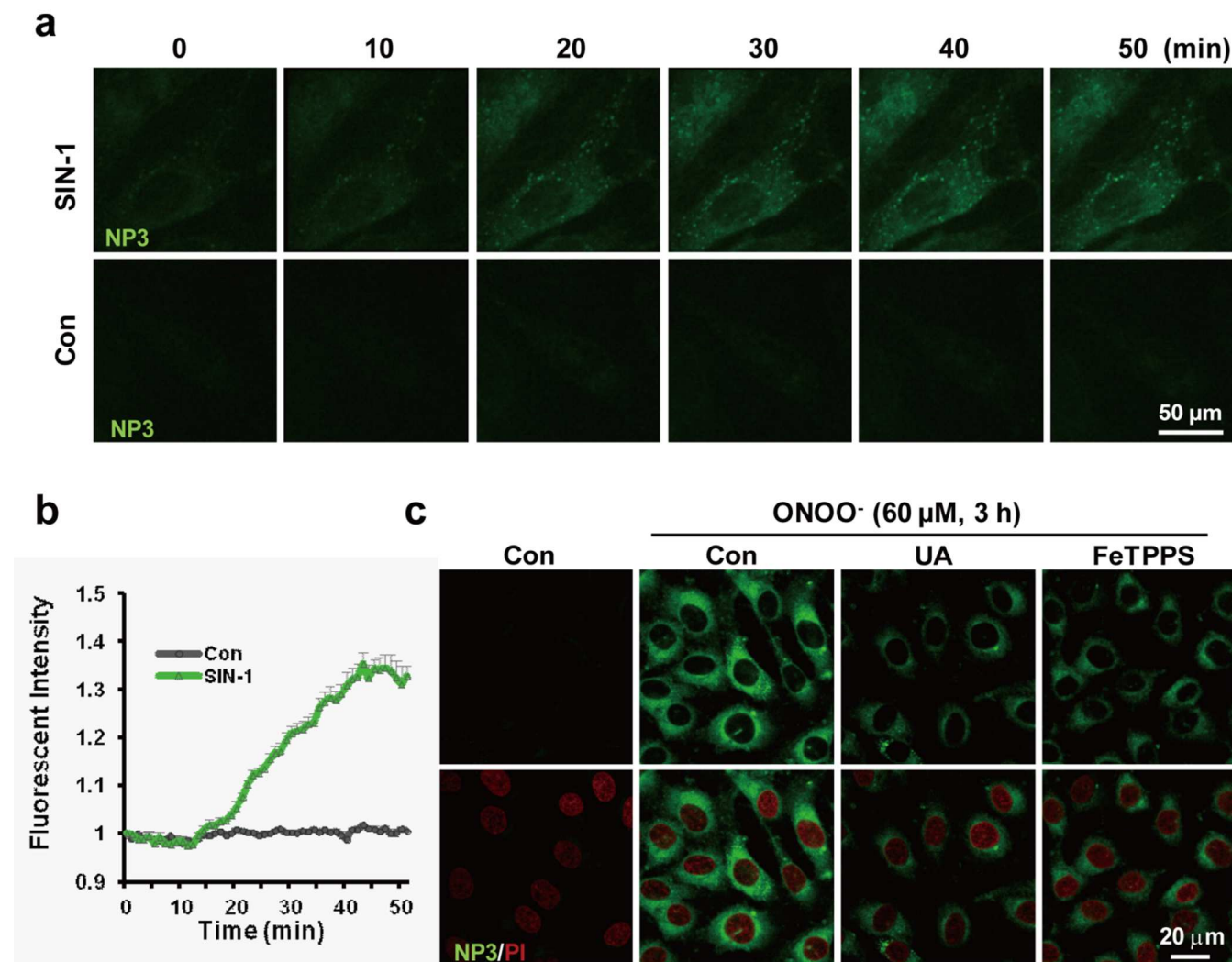


Figure 3. Characterization of ONOO⁻ formation by NP3 in endothelial cells upon nitrosative stress. (a) A time-lapse series of single confocal plane images taken from living EA.hy926 endothelial cells. The cells were seeded on glass-bottom 6-well plates overnight and then pre-incubated with NP3 (5.0 μ M) for 30 min, followed by stimulation with or without SIN-1 (0.5 mM). (b) Quantitative analysis of dynamic changes of NP3 fluorescence after SIN-1 (0.5 mM) treatment in (a). Data are presented as a densitometry ratio change compared with control. (c) Effects of ONOO⁻ scavengers uric acid (100 μ M) and FeTTPS (1 μ M) on changes in NP3 fluorescence in endothelial cells in the presence of ONOO⁻ (60 μ M). The ONOO⁻ scavengers were pre-incubated for 1 h prior to ONOO⁻ loading. PI counter staining indicates nuclear localization (red, λ_{ex} 543 nm, λ_{em} 560–615 nm). NP3 fluorescence was collected at 420–480 nm with λ_{ex} 405 nm.

Visualizing ONOO⁻ Fluxes in Endothelial Cells after Oxygen-Glucose Deprivation (OGD). Considerable evidence has indicated that ONOO⁻ overproduction in endothelial

cells mediates cellular damage during cerebral ischemia.^{46–48} Thus, it would be interesting if NP3 could help to identify dynamic changes of ONOO⁻ formation during endothelial

ischemic injury. As shown in Figure 4a, a time-dependent accumulation of NP3 fluorescence was observed in endothelial cells over 0.5 to 2 h following OGD exposure. A similar pattern of fluorescence was observed in HBMEC (Figure 4b). To elaborate the specificity of NP3 towards ONOO⁻ during OGD treatment, FeTTPS (1 μ M), the ONOO⁻ decomposition catalyst, blunted the elevation of NP3 fluorescence in OGD-treated endothelial cells (Figure 4c, Figure S18, S19), confirming that NP3 is specific for ONOO⁻ during OGD insult. ONOO⁻-mediated stress can also be initiated by early intracellular Ca²⁺ release and calmodulin activation.⁴⁹ To discern

whether the OGD-induced increase of NP3 fluorescence occurs in a Ca²⁺/Calmodulin-dependent manner, calmodulin inhibitors (W7 and melatonin) and a Ca²⁺-specific aminopolycarboxylic acid (1,2-bis(o-aminophenoxy)ethane-N,N,N',N'-tetraacetic acid, BAPTA) were used to bind Ca²⁺/Calmodulin signaling. As shown in Figure 4c and Figure S19, the OGD-induced increase of NP3 fluorescence was reduced in the presence of either the calmodulin inhibitor or BAPTA. Taken together, these results suggest that NP3 is a highly selective and specific probe for monitoring ONOO⁻ fluxes during ischemia.

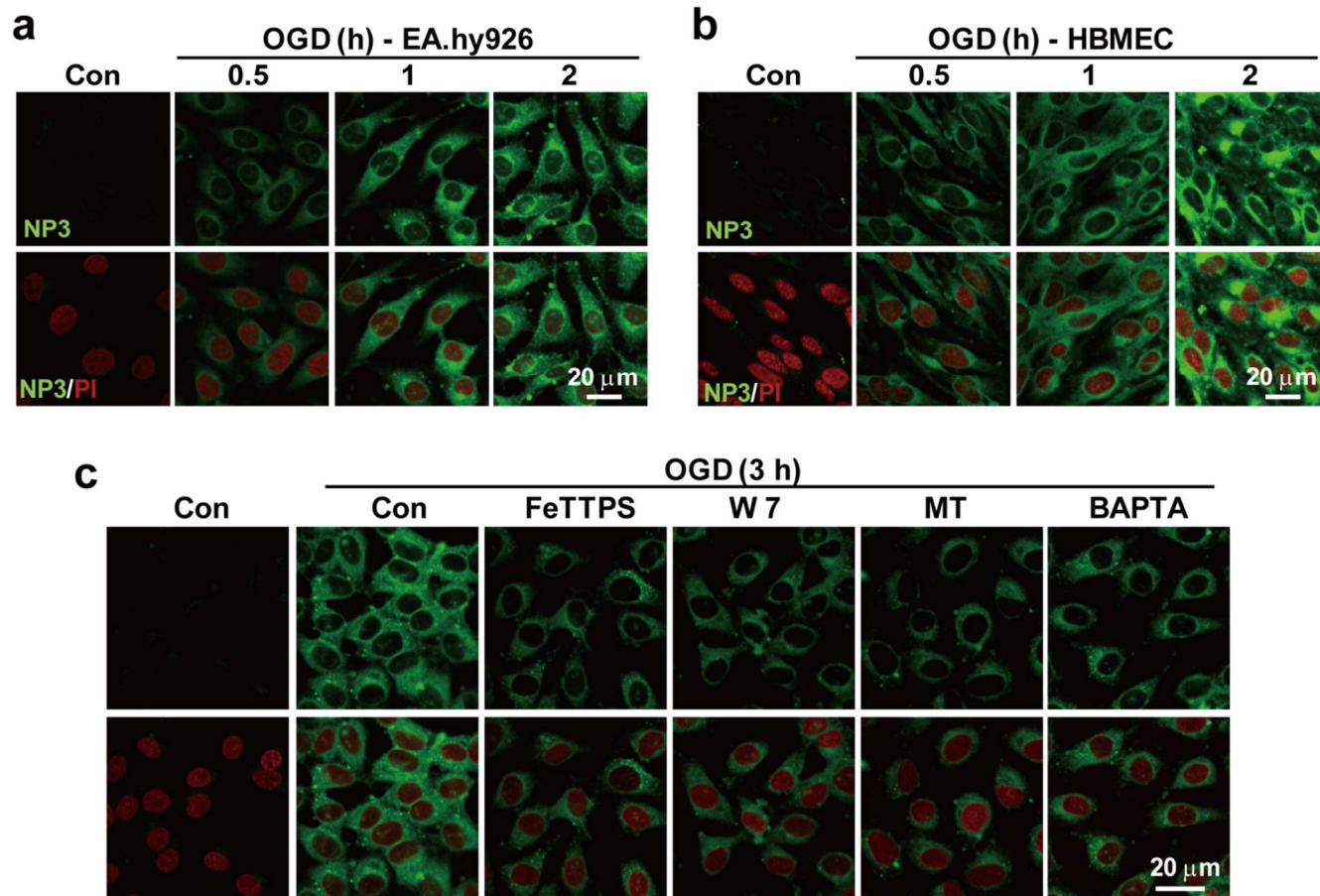


Figure 4. Characterization of ONOO⁻ formation using NP3 in endothelial cells upon OGD. The representative confocal images show time-dependent accumulation of NP3 fluorescence (green, λ_{ex} 405 nm, λ_{em} 420–480 nm) in EA.hy926 endothelial cells over 0.5 to 2 h following OGD exposure (a) as well as in human brain microvascular endothelial cells (HBMEC) in (b). PI counter staining indicated nuclear localization (red, λ_{ex} 543 nm, λ_{em} 560–615 nm). (c) The OGD-initiated NP3 fluorescence response to ONOO⁻ was modulated by suppressing ONOO⁻ formation. EA.hy926 endothelial cells were pretreated with FeTTPS (1 μ M), W7 (1 μ M), melatonin (10 μ M) and BAPTA (1 μ M) 1 h prior to OGD treatment to suppress the ONOO⁻ signal.

Real-time Monitoring of Vascular Peroxynitrite Fluxes with High Temporal and Spatial Resolution *In Vitro* In Live Cells. Mitochondria constitutes a primary locus for intracellular ONOO⁻ formation and target.⁵⁰ For example, modification of tyrosine residues by endogenous ONOO⁻ results in the inhibition of mitochondrial complex I.⁵¹ To further visualize the subcellular distribution of ONOO⁻ labeled by NP3 fluorescence, MitoRed (Invitrogen) was used to localize mitochondrial components in endothelial cells. NP3 fluorescence in control endothelial cells was undetected (Figure 5, Figure S20). Interestingly, consistent with MitoRed localization, elevated NP3 fluorescence in endothelial cells after OGD

was primarily observed localizing in the same components (Figure 5). Analysis of NP3 fluorescence (green) in mitochondrial components of endothelial cells revealed a significant elevation after 1 h of OGD, and continuous elevation could be observed after 2 h until at least 6 h (Figure 5, Figure S20). Moreover, coinciding with the reports that lysosome response is also associated with nitrosative stress,^{11,52} our results demonstrated that enhanced fluorescence partially located in the lysosomal compartment (Figure S21), suggesting the dynamic spatio-temporal coordination between ONOO⁻ and lysosomes. Similar changes in NP3 fluorescence were confirmed in HBMEC after OGD (Figure S22, S23). The results indicat-

ed that NP3 can monitor ONOO⁻ flux during ischemic injury. Accompanied by the increased NP3 fluorescence in mitochondria, as well as the spreading distribution in endothelial cell, ONOO⁻ accumulation challenged the endothelial cell and contributed to apoptosis, as shown by the Annexin V staining

(blue), in agreement with the results that ONOO⁻ could induce apoptosis (Figure S24). Thus, these collective data demonstrated that NP3 efficiently visualized the progressive ONOO⁻ fluxes in endothelial cells with excellent temporal and spatial ability.

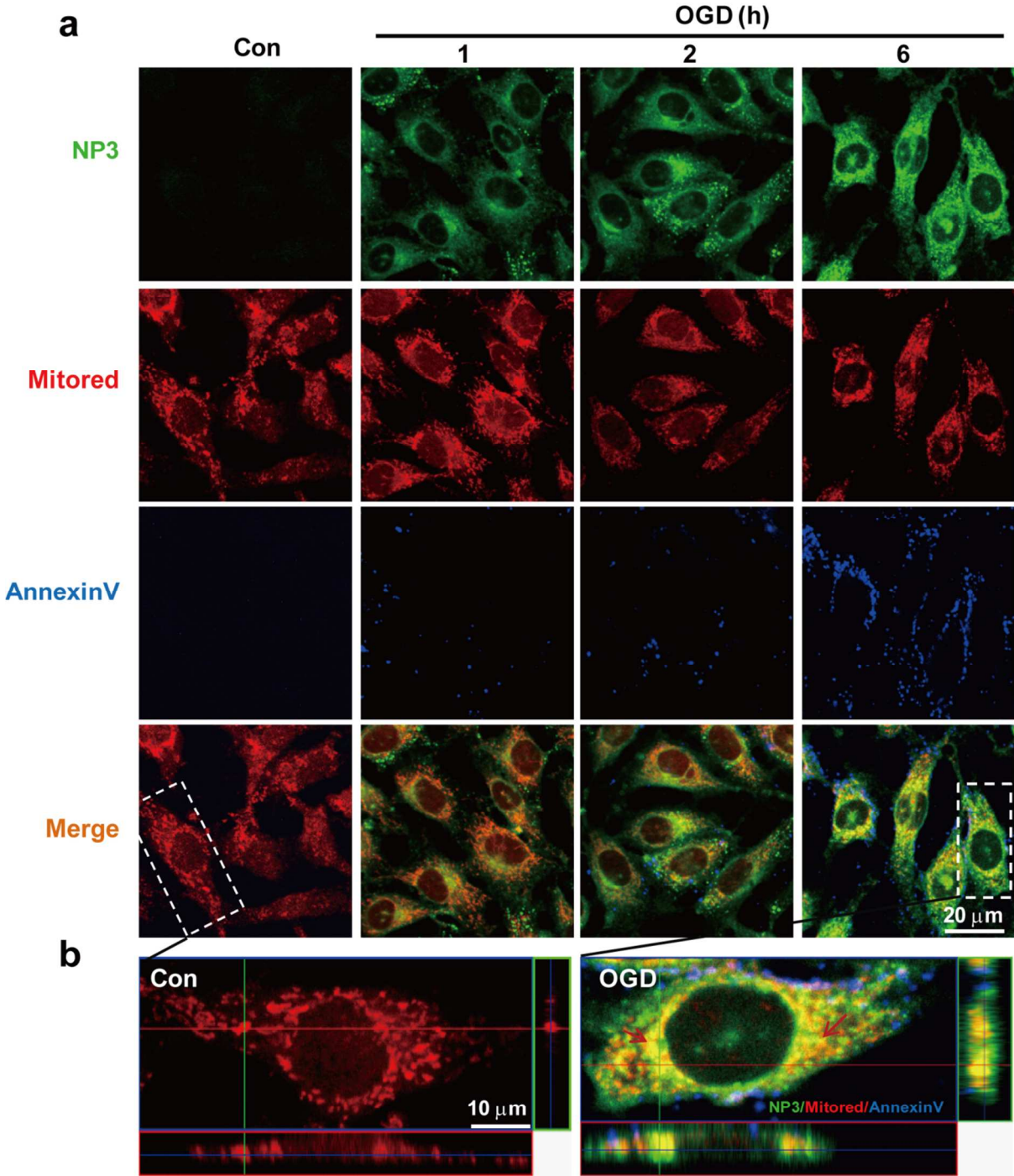


Figure 5. The distribution of NP3 fluorescence was examined by counterstaining with the mitochondria indicator Mitored after OGD. (a) Representative confocal images show the temporal changes of ONOO⁻-dependent NP3 fluorescence (green, λ_{ex} 405 nm, λ_{em} 420–480 nm) and Mitored (red, λ_{ex} 543 nm, λ_{em} 560–615 nm), as well as the apoptosis maker Annexin V (blue, λ_{ex} 488 nm, λ_{em} 505–550 nm), following OGD treatment. (b) Orthogonal projections onto the *x*-*z* (upper) and *y*-*z* (right) planes are shown to confirm the colocalization of NP3 and Mitored throughout the endothelial cells shown in (a) after ischemia injury. All images were captured using a Zeiss LSM 510 confocal microscope.

The MTT assay showed that NP3 did not exhibit cytotoxicity within 48 h except for such high concentrations as 150 and

200 μM (Figure S25). Moreover, the pretty low cytotoxicity of NP3 was confirmed by mitochondrial membrane potential-

sensing dye JC-1. Since the loss of mitochondrial transmembrane potential ($\Delta \Psi_m$) signals is a hallmark of mitochondrial dysfunction, cytotoxicity and apoptotic signaling,⁵³ we used JC-1 to further investigate the potential cytotoxic effects of NP3 on endothelial cells. No significant shift in JC-1 fluorescence from red to green was observed following NP3 treatment up to 100 μ M in EA.hy926 endothelial cells compared with control cells undergoing JC-1 staining (Figure S26). Thus, these results suggest that NP3 is nearly noncytotoxic up to 100 μ M in endothelial cells, implying the excellent biocompatibility for biological application, although further *in vivo* testing is necessary prior to application for clinical diagnosis.

Real-time Imaging of Endogenous Peroxynitrite Formation After Brain Microvessel Injury in Live Mice.

Combined with *in vivo* two-photon laser scanning microscopy (TPLSM), NP3 enabled visualization of the dynamic changes of neurovascular ONOO⁻ formation upon ischemia in live mice. The ischemia mice were modeled by Rose-Bengal-induced vascular occlusion⁵⁴ or laser irradiation-induced microvessel rupture.⁵⁵ The time series images in Figure 6 are individual frames from a continuous time-lapse movie. The dynamic elevation of local ONOO⁻ formation (arrows) in the microvessel indicated by strong NP3 fluorescence was effi-

ciently monitored over a recording period of 30 secs (Figure 6a, Movie S1). In contrast, no significant signal was observed in negative control experiments in which mice were modeled in the same way but not treated with NP3, indicating the capacity of NP3 for the *in vivo* tracking of ONOO⁻ fluxes during brain vascular damage (Figure S27).

Moreover, to provide another example of the *in vivo*-visualized ONOO⁻ flux enabled by NP3, real-time imaging of endogenous ONOO⁻ formation was performed in live mice suffering from laser irradiation-induced cerebrovascular rupture at the two-photon wavelength of 800 nm. As shown in Figure 6b, endogenous ONOO⁻ formation increased dramatically upon laser irradiation-mediated microvessel injury at 10 s point and remained at its highest fluorescent intensity for at least 30 secs (Figure 6b and c; Movie S2). Similar to our previously reported results that ischemia induced ONOO⁻ production based on indirect evidence from immunoblot or immunostaining,^{10,12} we observed laser irradiation-induced local ONOO⁻ formation in injured cerebral microvessels in live mice using the combination of *in vivo* TPLSM and probe NP3. More importantly, we were able to visualize the dynamic changes of ONOO⁻ formation in a temporal and spatial manner with high-resolution images in live mice.

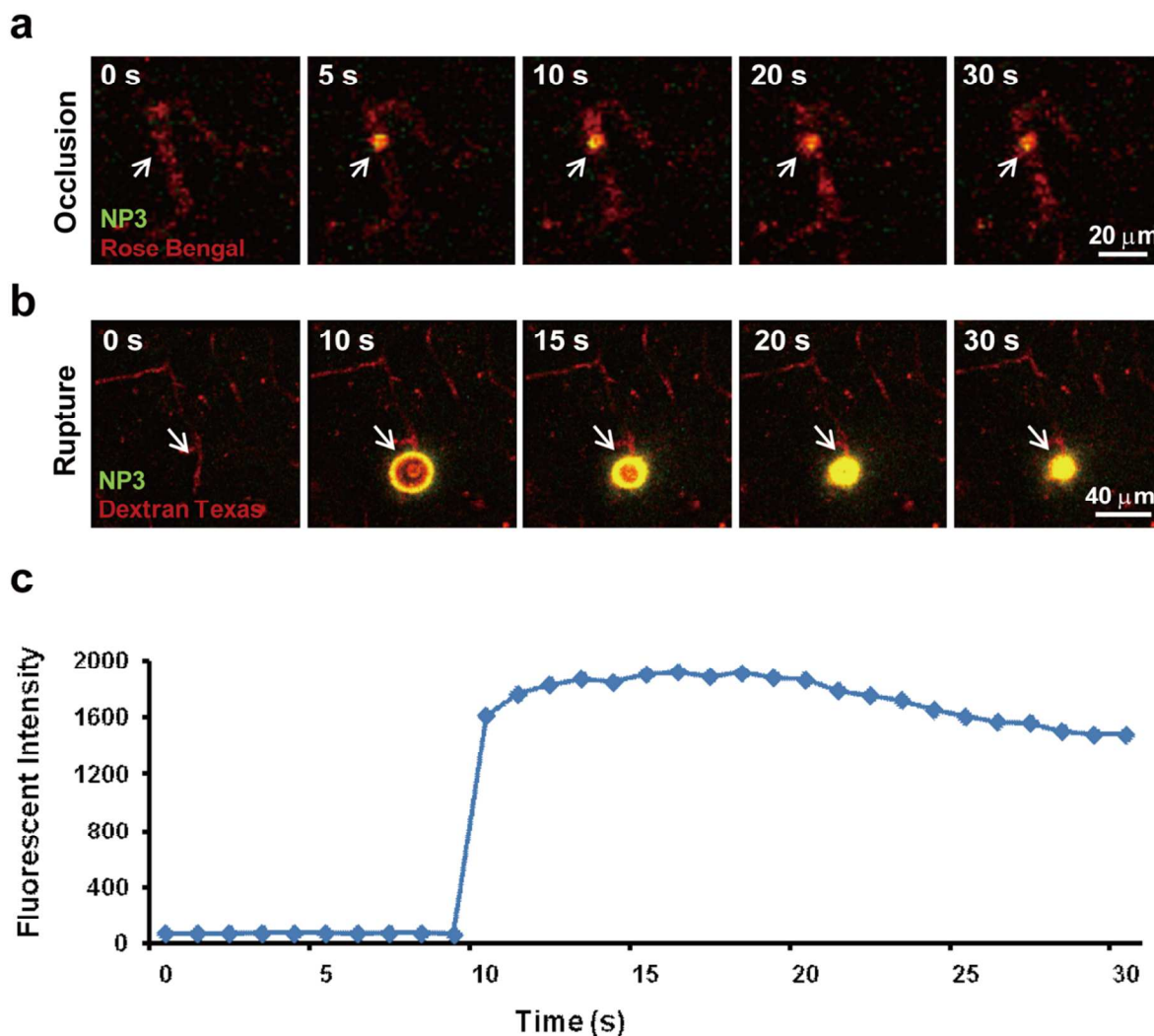


Figure 6. Real-time visualization of endogenous peroxynitrite fluxes after brain microvessel injury with a combination of **NP3** and *in vivo* two-photon laser scanning microscopy. For two-photon imaging, cortical brain vessels 10–15 μm in diameter and 100 μm below the cortical surface were selected for imaging. The time-series images in (a, b) are individual frames from a continuous time-lapse movie and show dynamic **NP3** fluorescence elevation (arrows) following Rose-Bengal-induced vascular occlusion (a) and laser irradiation-induced vascular rapture (b) in live mice. (c) The mean values of **NP3** fluorescence intensity from (b) were measured to quantify the progressive ONOO[−] formation in cerebrovessels after ischemia. Emission was collected at 420–480 nm for **NP3** fluorescence and 575–630 nm for dextran Texas or rose-Bengal upon excitation at 800 nm.

CONCLUSION

To conclude, by considering basic principles of probe and drug design, we developed a fluorescent probe with desired pharmacokinetic and photophysical properties suitable for imaging of ONOO[−] generation in both live cells and live animals. The probe, designed by blocking the ESPT process of the 2-(2'-hydroxyphenyl) benzothiazole fluorophore with a smart reaction trigger that is readily undergoing bioorthogonal and specific reaction with ONOO[−] in the biological contexts, features excellent specificity, high sensitivity, two-photon excitability and readily BBB penetrability. Application of this probe to track the *in situ* generation of ONOO[−] in the brain vasculature of live mice has provided the direct evidence that vascular occluding or laser irradiation would induce local ONOO[−] formation in injured cerebral microvessels. The probe should serve as a powerful imaging tool to explore ONOO[−] biology under a variety of pathological contexts *in vitro* and *in vivo*. Furthermore, the electronic and steric effects on probe sensitivity, and the significance of probe pharmacokinetic properties to its real-world application, as considered in this work, should be instructive for future probe design.

ASSOCIATED CONTENT

SUPPORTING INFORMATION

Synthesis, additional spectroscopic and confocal immunofluorescence data. These materials are available free of charge via the Internet at <http://pubs.acs.org>.

AUTHOR INFORMATION

Corresponding Author

*changhuahan@zju.edu.cn, huyz@zju.edu.cn and yhhu@mail.shcnc.ac.cn

Author Contributions

"X. L. and R. T contributed equally to this work.

Notes

The authors declare that they have no competing interests.

ACKNOWLEDGMENT

This work was supported in part by Projects of National Natural Science Foundations of China (81120108023, 81302748, 81300991).

ABBREVIATIONS

ONOO[−], peroxynitrite; ROS, reactive oxygen species; RNS, reactive nitrogen species; ESPT, excited state intramolecular proton transfer; BBB, blood-brain barrier.

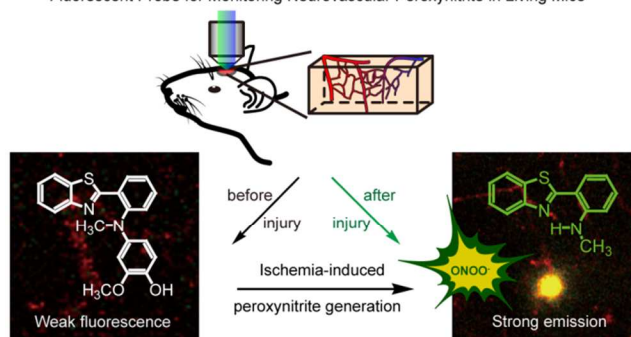
REFERENCES

- (1) Radi, R. *J. Biol. Chem.* **2013**, *288*, 26464.
- (2) Weidinger, A.; Kozlov, A. V. *Biomolecules* **2015**, *5*, 472.
- (3) Ascenzi, P.; di Masi, A.; Sciorati, C.; Clementi, E. *Biofactors* **2010**, *36*, 264.
- (4) Franco, M. C.; Estévez, A. G. *Cell. Mol. Life Sci.* **2014**, *71*, 3939.
- (5) Szabó, C.; Ischiropoulos, H.; Radi, R. *Nat. Rev. Drug Discov.* **2007**, *6*, 662.
- (6) Ferrer-Sueta, G.; Radi, R. *ACS Chem. Biol.* **2009**, *4*, 161.
- (7) Pacher, P.; Beckman, J. S.; Liaudet, L. *Physiol. Rev.* **2007**, *87*, 315.
- (8) Turko, I. V.; Murad, F. *Pharmacol. Rev.* **2002**, *54*, 619.
- (9) Wilcox, C. S.; Pearlman, A. *Pharmacol. Rev.* **2008**, *60*, 418.
- (10) Han, F.; Shirasaki, Y.; Fukunaga, K. *J. Neurochem.* **2006**, *99*, 97.
- (11) Han, F.; Chen, Y. X.; Lu, Y. M.; Huang, J. Y.; Zhang, G. S.; Tao, R. R.; Ji, Y. L.; Liao, M. H.; Fukunaga, K.; Qin, Z. H. *J. Pineal. Res.* **2011**, *51*, 124.
- (12) Tao, R. R.; Wang, H.; Hong, L. J.; Huang, J. Y.; Lu, Y. M.; Liao, M. H.; Ye, W. F.; Lu, N. N.; Zhu, D. Y.; Huang, Q.; Fukunaga, K.; Lou, Y. J.; Shoji, I.; Wilcox, C. X.; Lai, E. Y.; Han, F. *Antioxid. Redox Signal.* **2014**, *21*, 1.
- (13) Cross, A. H.; Manning, P. T.; Stern, M. K.; Misko, T. P. *J. Neuroimmunol.* **1997**, *80*, 121.
- (14) Nadler, A.; Schultz, C. *Angew. Chem. Int. Ed.* **2013**, *52*, 2408.
- (15) Ueno, T.; Nagano, T. *Nat. Methods* **2011**, *8*, 642.
- (16) Kobayashi, H.; Ogawa, M.; Alford, R.; Choyke, P. L.; Urano, Y. *Chem. Rev.* **2010**, *110*, 2620.
- (17) Yang, Y.; Zhao, Q.; Feng, W.; Li, F. *Chem. Rev.* **2013**, *113*, 192.
- (18) Domaille, D. W.; Que, E. L.; Chang, C. J. *Nat. Chem. Biol.* **2008**, *4*, 168.
- (19) Guo, Z.; Park, S.; Yoon, J.; Shin, I. *Chem. Soc. Rev.* **2014**, *43*, 16.
- (20) Denk, W.; Strickler, J. H.; Webb, W. W. *Science* **1990**, *248*, 73.
- (21) Wang, K. H.; Majewska, A.; Schummers, J.; Farley, B.; Hu, C.; Sur, M.; Tonegawa, S. *Cell* **2006**, *126*, 389–402.
- (22) Armon, T. I.; Horton, R. M.; Grigorova, I. L.; Cyster, J. G. *Nature* **2013**, *493*, 684.
- (23) Both APF and HPF are commercially available from Invitrogen.
- (24) Setsukinai, K.; Urano, Y.; Kakinuma, K.; Majima, H. J.; Nagano, T. *J. Biol. Chem.* **2003**, *278*, 3170.
- (25) Zhou, X.; Kwon, Y.; Kim, G.; Ryu, J. H.; Yoon, J. *Biosens. Bioelectron.* **2015**, *64*, 285.
- (26) Peng, T.; Wong, N. K.; Chen, X.; Chan, Y. K.; Ho, D. H.; Sun, Z.; Hu, J. J.; Shen, J.; El-Nezami, H.; Yang, D. *J. Am. Chem. Soc.* **2014**, *136*, 11728.
- (27) Hou, J. T.; Yang, J.; Li, K.; Liao, Y. X.; Yu, K. K.; Xie, Y. M.; Yu, X. Q. *Chem. Commun.* **2014**, *50*, 9947.
- (28) Chen, Z. J.; Ren, W.; Wright, Q. E.; Ai, H. W. *J. Am. Chem. Soc.* **2013**, *135*, 14940.
- (29) Lin, K. K.; Wu, S. C.; Hsu, K. M.; Hung, C. H.; Liaw, W. F.; Wang, Y. M. *Org. Lett.* **2013**, *15*, 4242.
- (30) Yu, F.; Li, P.; Wang, B.; Han, K. *J. Am. Chem. Soc.* **2013**, *135*, 7674.
- (31) Zhang, Q.; Zhu, Z.; Zheng, Y.; Cheng, J.; Zhang, N.; Long, Y. T.; Zheng, J.; Qian, X.; Yang, Y. *J. Am. Chem. Soc.* **2012**, *134*, 18479.
- (32) Yu, F.; Li, P.; Li, G.; Zhao, G.; Chu, T.; Han, K. *J. Am. Chem. Soc.* **2011**, *133*, 11030.
- (33) Peng, T.; Yang, D. *Org. Lett.* **2010**, *12*, 4932.

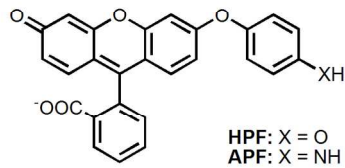
- (34) Zielonka, J.; Sikora, A.; Joseph, J.; Kalyanaraman, B. *J. Biol. Chem.* **2010**, 285, 14210.
- (35) Sun, Z. N.; Wang, H. L.; Liu, F. Q.; Chen, Y.; Tam, P. K.; Yang, D. *Org. Lett.* **2009**, 11, 1887.
- (36) Yang, D.; Wang, H. L.; Sun, Z. N.; Chung, N. W.; Shen, J. G. *J. Am. Chem. Soc.* **2006**, 128, 6004.
- (37) Ueno, T.; Urano, Y.; Kojima, H.; Nagano, T. *J. Am. Chem. Soc.* **2006**, 128, 10640.
- (38) Lou, Z.; Li, P.; Han, K. *Acc. Chem. Res.* **2015**, 48, 1358.
- (39) Chan, J.; Dodani, S. C.; Chang, C. J. *Nat. Chem.* **2012**, 4, 973.
- (40) Lemke, E. A.; Schultz, C. *Nat. Chem. Biol.* **2011**, 7, 480.
- (41) Mathis, C. A.; Wang, Y.; Holt, D. P.; Huang, G. F.; Debnath, M. L.; Klunk, W. E. *J. Med. Chem.* **2003**, 46, 2740.
- (42) Woolfe, G. J.; Melzig, M.; Schneider, S.; Dorr, F. *Chemical Physics* **1983**, 77, 213.
- (43) So, P.; Two-photon Fluorescence Light Microscopy, Encyclopedia of Life Sciences, 2002, Macmillan Publishers Ltd, Nature Publishing Group
- (44) Albota, M. A.; Xu, C.; Webb, W. W. *Appl. Opt.* **1998**, 37, 7352.
- (45) Data in agreement with reported: Pierens, G. K.; Venkatachalam, T. K.; Reutens, D. *Magn. Reson. Chem.* **2014**, 52, 453.
- (46) Dugo, L.; Serraino, I.; Fulia, F.; De Sarro, A.; Caputi, A. P.; Cuzzocrea, S. *J. Pineal. Res.* **2001**, 31, 76.
- (47) Teixeira, A.; Morfim, M. P.; de Cordova, C. A.; Charão, C. C.; de Lima, V. R.; Creczynski-Pasa, T. B. *J. Pineal. Res.* **2003**, 35, 262.
- (48) Yin, J.; Liu, Y. H.; Xu, Y. F.; Zhang, Y. J.; Chen, J. G.; Shu, B. H.; Wang, J. Z. *J. Pineal. Res.* **2006**, 41, 124.
- (49) Han, F.; Tao, R. R.; Zhang, G. S.; Lu, Y. M.; Liu, L. L.; Chen, Y. X.; Lou, Y. J.; Fukunaga, K.; Hong, Z. H. *J. Pineal. Res.* **2011**, 50, 281.
- (50) Indo, H. P.; Yen, H. C.; Nakanishi, I.; Matsumoto, K.; Tamura, M.; Nagano, Y.; Matsui, H.; Gusev, O.; Cornette, R.; Okuda, T.; Minamiyama, Y.; Ichikawa, H.; Suenaga, S.; Oki, M.; Sato, T.; Oza-wa, T.; Clair, D. K.; Majima, H. J. *J. Clin. Biochem. Nutr.* **2015**, 56, 1.
- (51) Bharath, S.; Andersen, J. K. *Antioxid. Redox. Signal.* **2005**, 7, 900.
- (52) Tripathi, D. N.; Chowdhury, R.; Trudel, L. J.; Tee, A. R.; Slack, R. S.; Walker, C. L.; Wogan, G. N. *Proc. Natl. Acad. Sci. USA* **2013**, 110, E2950.
- (53) Liu, Q. B.; Liu, L. L.; Lu, Y. M.; Tao, R. R.; Huang, J. Y.; Han, F.; Lou, Y. J. *Toxicol. Appl. Pharmacol.* **2010**, 244, 374.
- (54) Schaffer, C. B.; Friedman, B.; Nishimura, N.; Schroeder, L. F.; Tsai, P. S.; Ebner, F. F.; Lyden, P. D.; Kleinfeld, D. *PLoS Biol.* **2006**, 4, e22.
- (55) Nishimura, N.; Schaffer, C. B.; Friedman, B.; Tsai, P. S.; Lyden, P. D.; Kleinfeld, D. *Nat. Methods* **2006**, 3, 99.

Table of Contents

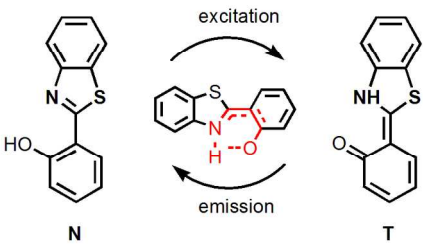
Fluorescent Probe for Monitoring Neurovascular Peroxynitrite in Living Mice



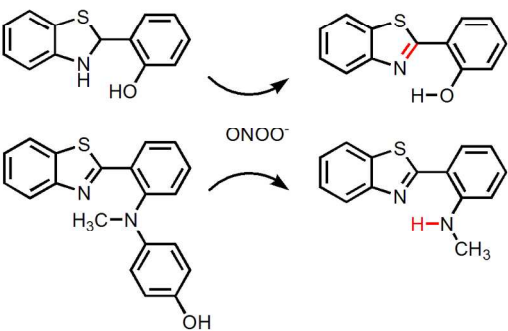
Structures of HPF and APF



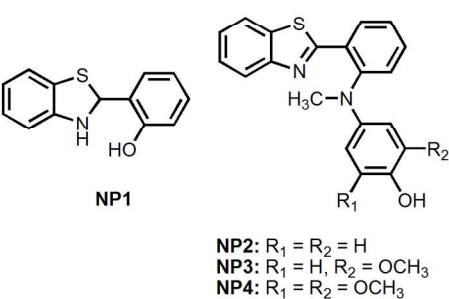
ESIPT effect of benzothiazole dyes



Design philosophy



Structures of ONOO⁻ probes



164x119mm (300 x 300 DPI)

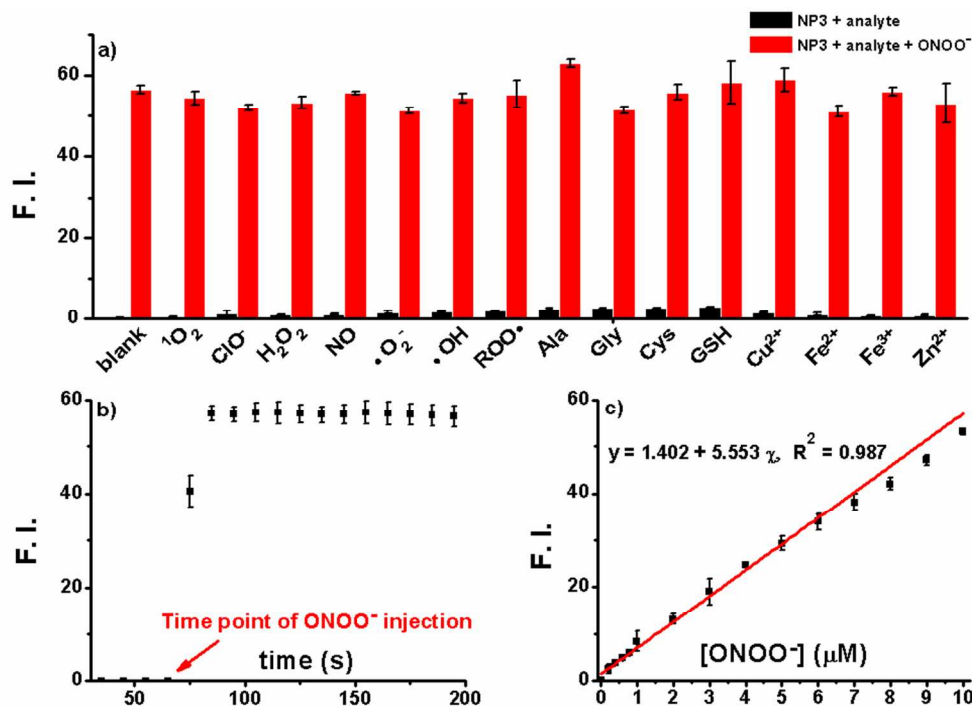


Figure 2. Characterization of the fluorescent response of NP3 towards ONOO^- . (a) Fluorescent responses of NP3 (5 μM) towards various analytes (10 μM). Data shown represent the fluorescent intensity at 470 nm 30 min after the addition of various analytes. (b) ONOO^- (finally concentration 10 μM) was quickly injected into a solution of NP3 (final concentration 5 μM) and the fluorescent intensity at 470 nm was plotted against time. (c) Fluorescence enhancement of NP3 (5 μM) at 470 nm as a function of ONOO^- (0–10 μM) after 15 min of reaction. All the data were acquired in PBS (10 mM, pH 7.4) with excitation 375 nm.

83x59mm (300 x 300 DPI)

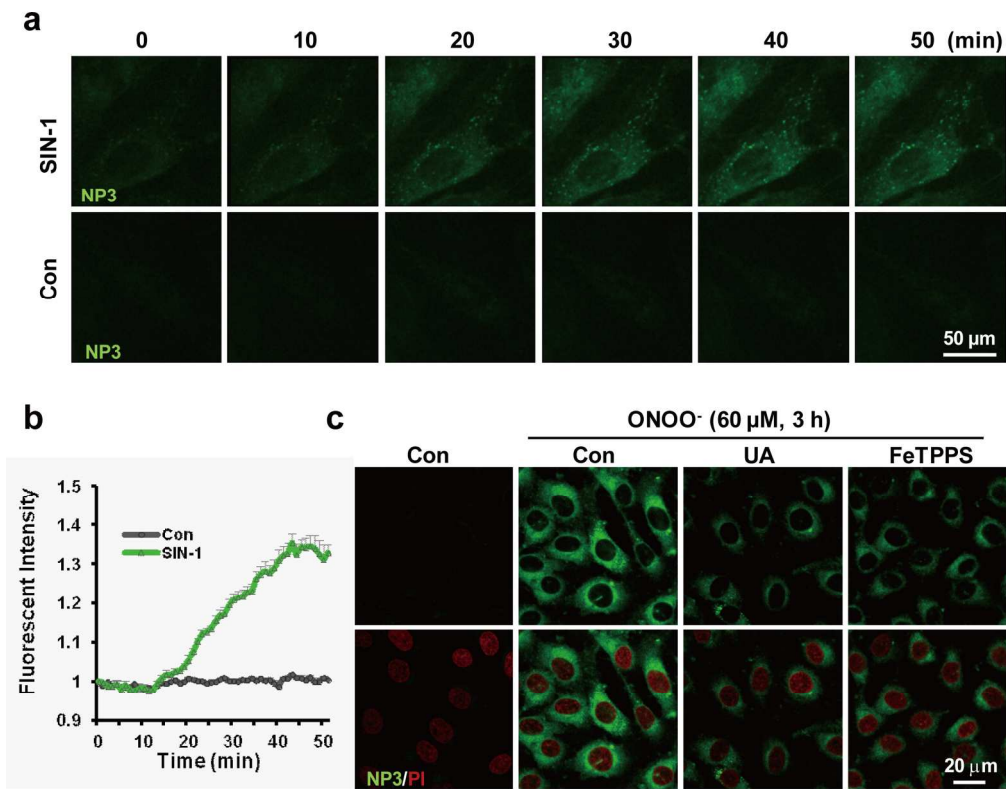


Figure 3. Characterization of ONOO⁻ formation by NP3 in endothelial cells upon nitrosative stress. (a) A time-lapse series of single confocal plane images taken from living EA.hy926 endothelial cells. The cells were seeded on glass-bottom 6-well plates overnight and then pre-incubated with NP3 (5.0 μM) for 30 min, followed by stimulation with or without SIN-1 (0.5 mM). (b) Quantitative analysis of dynamic changes of NP3 fluorescence after SIN-1 (0.5 mM) treatment in (a). Data are presented as a densitometry ratio change compared with control. (c) Effects of ONOO⁻ scavengers uric acid (100 μM) and FeTPPS (1 μM) on changes in NP3 fluorescence in endothelial cells in the presence of ONOO⁻ (60 μM). The ONOO⁻ scavengers were preincubated for 1 h prior to ONOO⁻ loading. PI counter staining indicates nuclear localization (red, λ_{ex} 543 nm, λ_{em} 560-615 nm). NP3 fluorescence was collected at 420-480 nm with λ_{ex} 405 nm.

176x139mm (300 x 300 DPI)

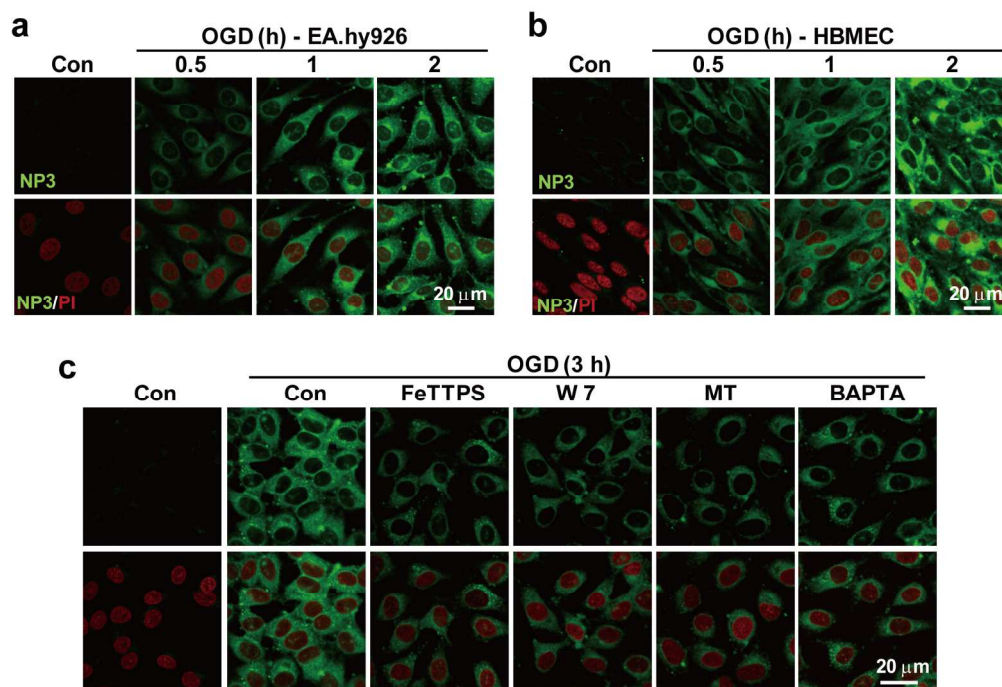


Figure 4. Characterization of ONOO⁻ formation using NP3 in endothelial cells upon OGD. The representative confocal images show time-dependent accumulation of NP3 fluorescence (green, λ_{ex} 405 nm, λ_{em} 420-480 nm) in EA.hy926 endothelial cells over 0.5 to 2 h following OGD exposure (a) as well as in human brain microvascular endothelial cells (HBMEC) in (b). PI counter staining indicated nuclear localization (red, λ_{ex} 543 nm, λ_{em} 560-615 nm). (c) The OGD-initiated NP3 fluorescence response to ONOO⁻ was modulated by suppressing ONOO⁻ formation. EA.hy926 endothelial cells were pretreated with FeTTPS (1 μ M), W7 (1 μ M), melatonin (10 μ M) and BAPTA (1 μ M) 1 h prior to OGD treatment to suppress the ONOO⁻ signal.

175x119mm (300 x 300 DPI)

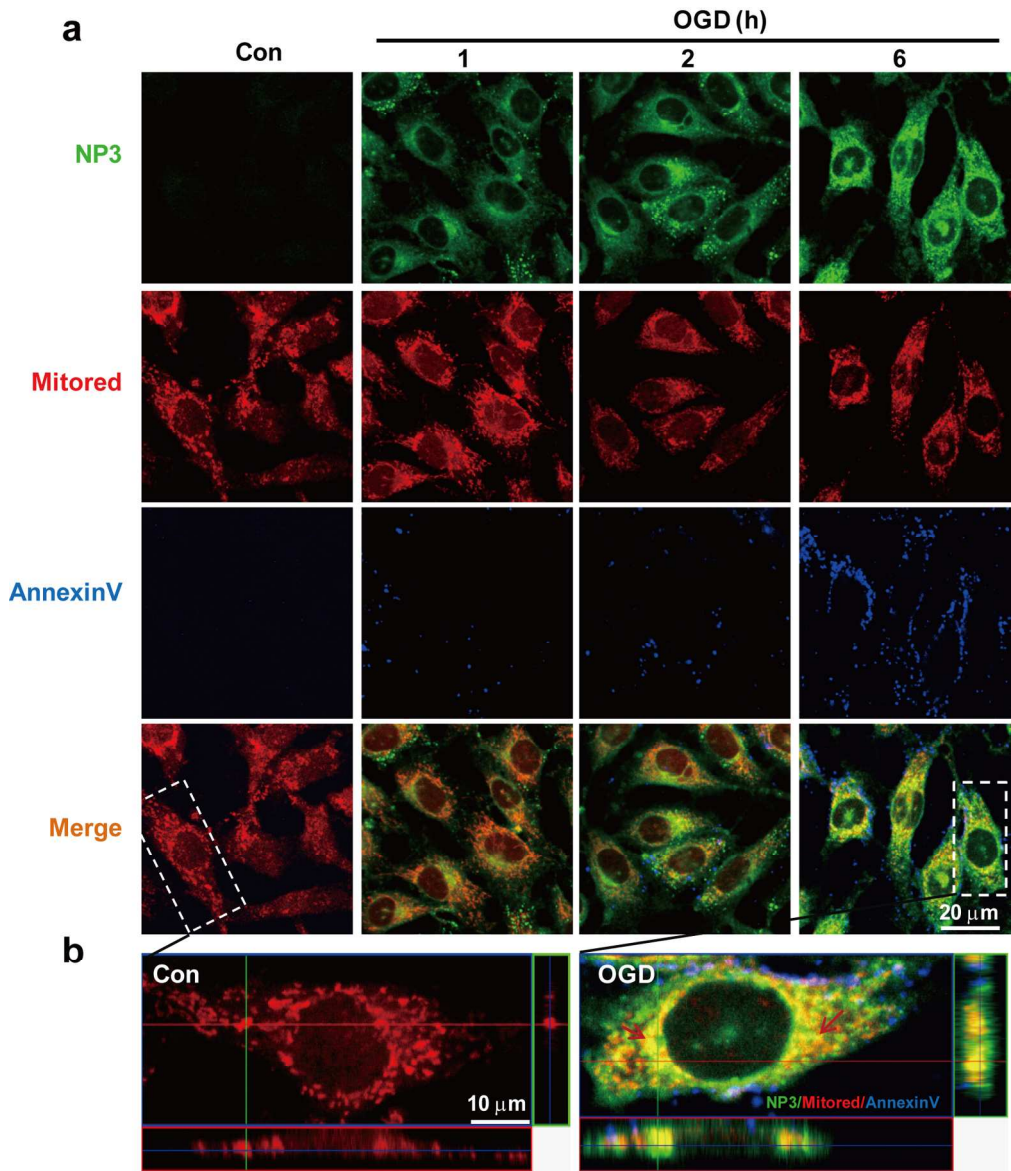


Figure 5. The distribution of NP3 fluorescence was examined by counterstaining with the mitochondria indicator MitoRed after OGD. (a) Representative confocal images show the temporal changes of ONOO--dependent NP3 fluorescence (green, λ_{ex} 405 nm, λ_{em} 420-480 nm) and MitoRed (red, λ_{ex} 543 nm, λ_{em} 560-615 nm), as well as the apoptosis marker Annexin V (blue, λ_{ex} 488 nm, λ_{em} 505-550 nm), following OGD treatment. (b) Orthogonal projections onto the x-z (upper) and y-z (right) planes are shown to confirm the colocalization of NP3 and MitoRed throughout the endothelial cells shown in (a) after ischemia injury. All images were captured using a Zeiss LSM 510 confocal microscope.

159x185mm (300 x 300 DPI)

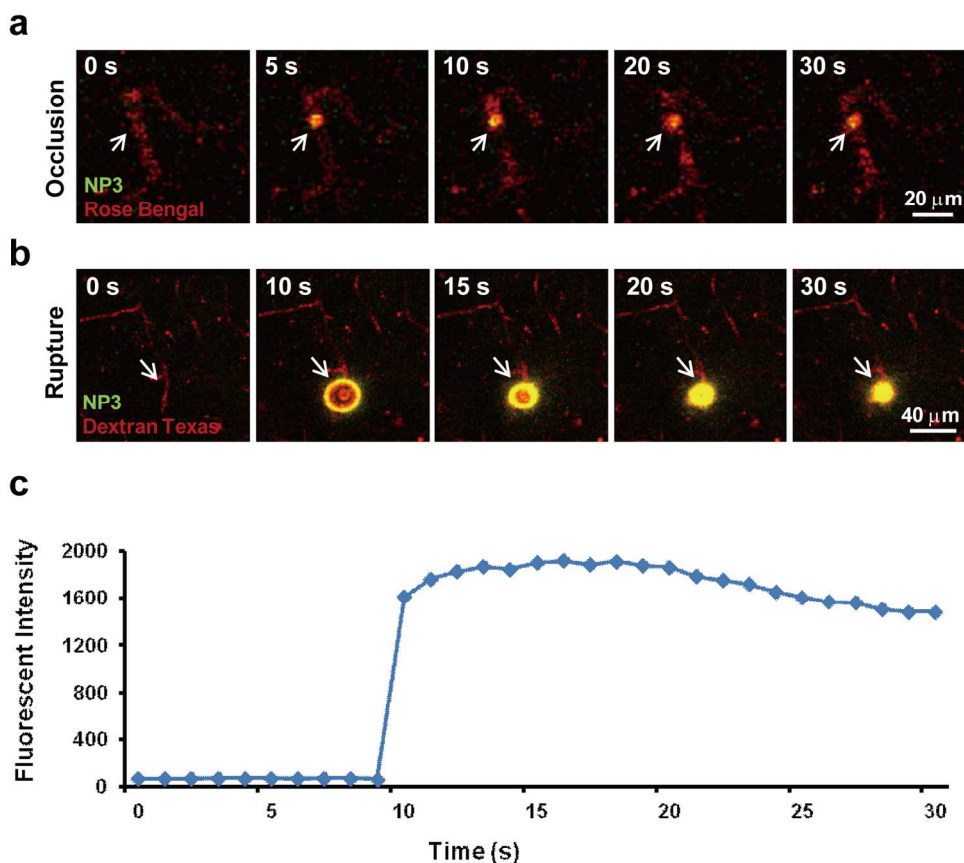


Figure 6. Real-time visualization of endogenous peroxynitrite fluxes after brain microvessel injury with a combination of NP3 and in vivo two-photon laser scanning microscopy. For two-photon imaging, cortical brain vessels 10~15 μ m in diameter and 100 μ m below the cortical surface were selected for imaging. The time-series images in (a, b) are individual frames from a continuous time-lapse movie and show dynamic NP3 fluorescence elevation (arrows) following Rose-Bengal-induced vascular occlusion (a) and laser irradiation-induced vascular rupture (b) in live mice. (c) The mean values of NP3 fluorescence intensity from (b) were measured to quantify the progressive ONOO⁻ formation in cerebrovessels after ischemia. Emission was collected at 420-480 nm for NP3 fluorescence and 575-630 nm for dextran Texas or rose-Bengal upon excitation at 800 nm.

161x145mm (300 x 300 DPI)